A computer model of dorsal cochlear nucleus pyramidal cells: Intrinsic membrane properties

Michael J. Hewitt and Ray Meddis
Speech and Hearing Laboratory, Department of Human Sciences, University of Technology, Loughborough LE11 3TU, United Kingdom

(Received 3 March 1994; accepted for publication 1 December 1994)

Manis [P. B. Manis, J. Neurosci. **10**, 2338–2351 (1990)] studied "simple spiking," pyramidal cells of the dorsal cochlear nucleus (DCN) maintained *in vitro*. Response profiles to hyperpolarizing and depolarizing current pulses were generated. Hyperpolarization of the cell membrane followed by depolarization produced markedly different response profiles from those generated when no prehyperpolarization was imposed. By manipulating the magnitude of the hyperpolarizing and depolarizing pulses, "chopper," "pauser" and "build-up" response patterns, similar to those *in vivo*, could be generated by individual cells. Manis concluded that the different response profiles resulted from the modulation of intrinsic membrane conductances by the prehyperpolarizing pulses. Here a computer model is used to show that (a) steady-state hyperpolarization can influence cell responding to subsequent depolarization in a manner consistent with the data reported by Manis; and (b) the effects reported can be generated by the addition of a modeled transient potassium conductance to the standard Hodgkin–Huxley model of spike generation [A. L. Hodgkin and A. F. Huxley, J. Physiol. **117**, 500–544 (1952)]. The model will be of use to those who wish to consider the role of various excitatory and inhibitory inputs to pyramidal cells and to establish their functional role within the DCN.

PACS numbers: 43.64.Qh, 43.64.Bt

INTRODUCTION

This article is one of a series of computer modeling studies aimed at understanding the mechanisms that underlie information processing in the auditory brain stem. Previous studies have focused on ventral cochlear nucleus stellate cells (Hewitt *et al.*, 1992; Hewitt and Meddis, 1993; see also Arle and Kim, 1991; Banks and Sachs, 1991; Ghoshal *et al.*, 1992) and the inferior colliculus (Hewitt and Meddis, 1994). Here, we model the intrinsic membrane conductances that may underpin the complex response properties of dorsal cochlear nucleus (DCN) pyramidal (or fusiform) cells.

The pyramidal cells of the mammalian DCN show a variety of post stimulus time histogram profiles in response to acoustic stimuli. "Chopper," "buildup," and "pauser" response types can all be generated by individual units depending on stimulus conditions (Goldberg and Brownell, 1973; Godfrey *et al.*, 1975; Adams, 1976; Rhode and Kettner, 1987).

Early theorists hypothesized that such response types could be explained within a framework of synaptic excitation and inhibition (e.g., Greenwood and Maruyama, 1965; Kane, 1974). For example, a pauser profile could result from delayed inhibition which is eventually superseded by excitation. In support of this notion, anatomical and physiological studies of pyramidal cells show that they receive both excitatory and inhibitory inputs (e.g., Smith and Rhode, 1985; Hirsch and Oertel, 1988b). However, intracellular recordings of DCN cells have shown that silent periods in response to acoustic stimulation are not necessarily associated with hyperpolarization of the cell membrane (e.g., Britt and Starr, 1976; Romand, 1978). More recently, Rhode and colleagues (1983, 1986) presented data to suggest that the resting potential of the cell membrane plays an important role in the generation of DCN cell responses. Manis (1990) tested this idea experimentally and produced data to support an alternative theory to that previously stated.

Manis (1990) made intracellular recordings from DCN pyramidal cells maintained in an *in vitro* brain slice preparation. He studied the intrinsic electrical properties of the cells by measuring responses to injected depolarizing and hyperpolarizing current pulses of different magnitudes. The main effect reported was that steady-state hyperpolarization altered cell responding to subsequent depolarization. By manipulating the magnitude of hyperpolarization and depolarization, he was able to produce spike response patterns that resembled those found *in vivo* in response to acoustic stimuli.

Manis considered the characteristics of the voltage-dependent membrane conductance(s) that might underlie the generation of the different response patterns. One scenario required the existence of a transient potassium conductance. Such a conductance is found in other neuronal preparations and has been shown to affect cell firing patterns in the way required here (e.g., Connor and Stevens, 1971). Furthermore, transient potassium conductances are sensitive to the drug 4-AP; similar 4-AP sensitive conductances have been found in DCN cells (Hirsch and Oertel, 1988b).

Finally, Manis (1990) concluded that the transient potassium conductance was the most parsimonious explanation for the observed response profiles. However, this was only conjecture and he did not demonstrate it directly. In this paper we provide evidence to corroborate the experimental findings. More specifically, we show using a computer model

 0001-4966/95/97(4)/2405/9/$6.00

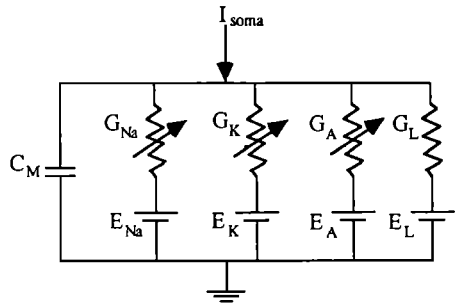

FIG. 1. Equivalent electrical circuit for model neuron. Conductances G_K, G_{Na}, and G_A vary with time and membrane potential; I_{soma} represents the magnitude of injected current; other components are constant.

that (a) steady-state hyperpolarization can influence cell responding to subsequent depolarization in a manner consistent with the data reported by Manis; and (b) the effects reported can be generated by the addition of a modeled transient potassium conductance to a standard Hodgkin–Huxley (1952) model of spike generation.

The working model provides a detailed description of the mechanisms that may operate at the site of spike generation in DCN pyramidal cells. It will be of use to those who wish to consider the complex synaptic inputs to this class of DCN cells in order to generate and test hypotheses concerning their functional role within the DCN.

I. THE MODEL

The model of Hodgkin and Huxley (1952) was originally proposed to account for the generation of single action potentials in squid giant axon. Although the model suffers from some specific shortcomings (see MacGregor, 1987), it remains the most commonly used formulation in which to cast voltage-clamp data from both invertebrate and vertebrate preparations.

Below we outline the basic model and present modifications that enable us to replicate the salient features of the data presented by Manis (1990). The final model is a hybrid: The basic Hodgkin–Huxley model (a sodium conductance and a delayed rectifier potassium conductance) was implemented using the equations given by Banks and Sachs (1991); the transient potassium conductance was implemented using the equations given by Connor *et al.* (1977).

Figure 1 shows the equivalent electrical circuit of the proposed model. The principal differential equation describing the circuit is

$$I(t)=C_M\frac{dV}{dT}+g_L(V-E_L)+g_{Na}(V-E_{Na})+g_K(V-E_K)+g_A(V-E_A)+I_{soma}. \quad (1)$$

The model consists of three voltage-dependent conductances (g_{Na}, g_K, and g_A) together with a fixed leakage conductance (g_L) and capacitance (C_M). The value of the leakage conductance is commonly used to set the resting potential of the cell.

The original Hodgkin–Huxley model described the sodium and potassium conductances, g_{Na} and g_K, respectively, as

$$g_{Na}=\bar{g}_{Na}m^3(V,t)h(V,t) \quad (2)$$

and

$$g_k=\bar{g}_k n^4(V,t). \quad (3)$$

Here g_{Na} is defined in terms of two hypothetical continuous functions h and m, and g_K is defined in terms of the function n. These functions were conceptualized by Hodgkin and Huxley (1952) in terms of gating particles, moving between open and closed states.

All three functions are given by rate equations guided by α and β parameters. These rate-governing α and β parameters are represented by experimentally determined functions of membrane potential, V. The equations and parameters describing these functions are provided in the Appendix. Following the practice of Connor *et al.* (1977) and Banks and Sachs (1991), m, h, and n were adjusted to give realistic spike threshold values.

The transient potassium conductance g_A was implemented as stated in Connor *et al.* (1977):

$$g_A=\bar{g}_A A^3(V,t)B(V,t). \quad (4)$$

The functions A and B (see the Appendix) have the same functional significance as the m and h factors of the sodium conductance system. Both functions were shifted along the voltage axis to provide acceptable fits to the physiological data. These details are documented in the Appendix. The model equations were programmed in ANSI-C using the modified Euler method. A step integration size of 20 μs was used.[1]

II. RESULTS

Below we compare model output to the data of Manis (1990; see also Hirsch and Oertel, 1988a). Manis made intracellular recordings from 72 guinea pig cells located in the DCN. Recordings from 83% of cells (60/72) formed the basis of the reported data. These cells responded to depolarizing current pulses with simple, all-or-none action potentials; the remainder, which showed more complex spiking behavior, were not discussed further. Eleven cells were marked with dye. Ten of these were later identified as pyramidal cells (all stained cells were simple spiking cells).

About one-half of the recorded cells had little or no firing activity in the absence of stimulating pulses; the remainder fired at rates of between 30 and 50 Hz. In the latter case, a hyperpolarizing current was used to silence the firing activity to facilitate the analysis of current–voltage relationships. The standard parameter set used for the model simulations reported below were selected to give a model cell with no firing activity in the absence of stimulating pulses. The resting potential of the model cell was set to −60 mV, which is within the range of resting levels reported for simple spiking DCN cells (Hirsch and Oertel, 1988a; Manis, 1990).

Manis (1990) used trace recordings from different cells to demonstrate the properties of DCN pyramidal cells. Model

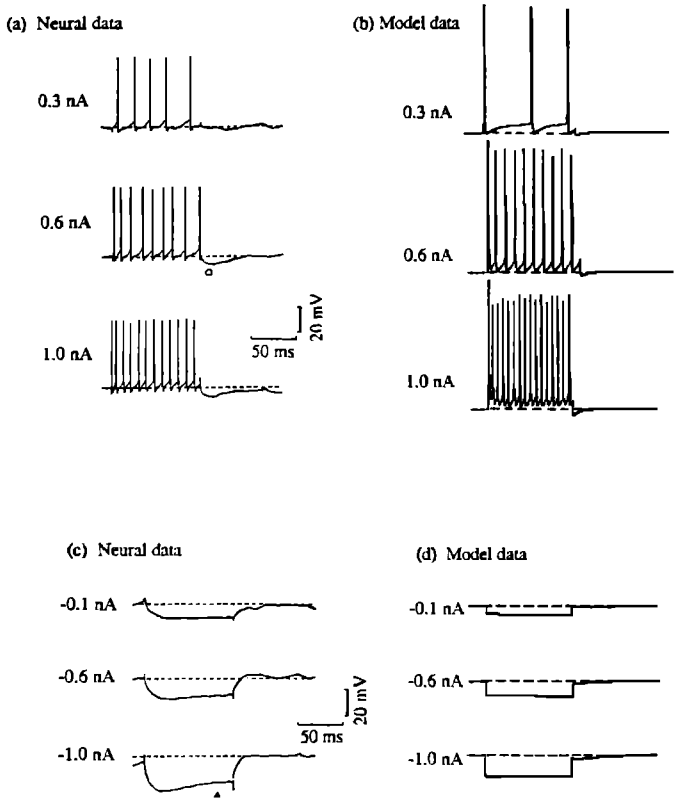

FIG. 2. Depolarizing and hyperpolarizing current pulses. (a) and (c) redrawn from Manis (1990, Fig. 2). Open circle denotes afterhyperpolarization; open triangle points to rise in membrane potential. (b) and (d) from model.

parameters could be tuned to match individual cell responses quantitatively. However, we chose to present data using a fixed parameter set. This data replicates, at a qualitative level, that presented by Manis. In Sec. II E, below, we identify the parameters of the model that most influence its output.

A. Responses to injected current

Depolarizing current pulses applied intracellularly to impaled DCN cells typically produce regular trains of stereotyped spikes (Manis, 1990; Hirsch and Oertel, 1988a). Figure 2(a) shows data reported by Manis (1990). The rate of firing increases with increases in current strength (quantified later). Each action potential is about 60 mV in height and shows a two-component recovery phase, with an initial fast component followed by a slower one. At the offset of large depolarizations (>0.6 nA), a notable afterpolarization occurs. Hyperpolarizing current pulses [Fig. 2(c)] produce almost exponential changes in membrane potential at onset and offset (Manis, 1990; Hirsch and Oertel, 1988a). For pulses more negative than −0.6 nA a small rise in membrane potential is evident after about 20 ms.

Figure 2(b) and (d) shows the corresponding model outputs. The main features of the neural data are replicated, qualitatively at least, by the model; they are (a) an increase in firing rate with increases in the magnitude of depolarizing pulses, (b) hyperpolarization at the offset of large depolarizing pulses e.g., Fig. 2(b), 1.0 nA, (c) increase in membrane potential below resting with increases in magnitude of hyperpolarizing current pulses, and (d) evidence of a small sag in membrane potential for large hyperpolarizing pulses, e.g., Fig. 2(d), −1.0 nA.

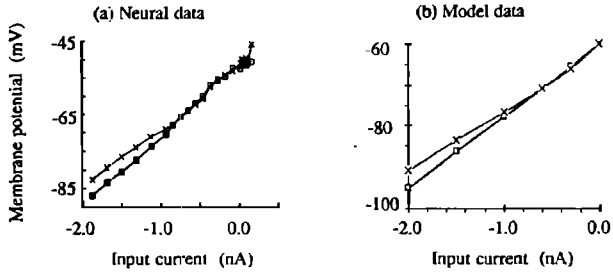

FIG. 3. Current–voltage relationships. Open squares denote membrane potential at pulse onset; crosses denote potential just before pulse offset. (a) Neural data redrawn from Manis (1990, Fig. 3 panel A). (b) Model data.

Certain other features present in the experimental data are absent from model traces and will be discussed later in the paper. For example, the clear two-component postspike recovery process of the neural data is not replicated by the model. Second, model spike heights are about 20 mV greater than their neural counterparts. Third, the model shows baseline depolarization at 1.0 nA which does not appear in the data reported by Manis [but is apparent in Hirsch and Oertel's (1988a) data, Fig. 4]. Finally, model onset responses to hyperpolarizing pulses are too fast, and do not follow the slower exponentia' course shown by the neural data.

B. Current–voltage relationships

Manis constructed current–voltage relationships from cell responses to hyperpo'arizing current pulses. One example is presented in Fig. 3(a). Two traces are shown, one to depict the membrane potential shortly after pulse onset and the other to show membrane potential just before pulse offset. Near pulse onset, the input/output characteristics are approximately linear. Deviation from linearity occurs for the responses measured just before pulse offset. This relates to the sag in membrane potential noted in Fig. 2. Figure 3(b) shows similar responses which were obtained from the model.

Current–voltage relationships for depolarizing pulses are difficult to assess due to contamination of traces by action potentials. However, for small depolarizing pulses (<0.1 nA) this is not too problematic. In these cases the neural traces show evidence of a further nonlinearity in the form of a small inward rectification (see neural data in Fig. 3). This was also reported by Hirsch and Oertel (1988a) and has been attributed to a slow voltage-dependent sodium current. This particular nonlinearity is not replicated by the current model.

C. Discharge rate versus current magnitude

Manis (1990) found that the average discharge rate of pyramidal cells increased monotonically with increases in current magnitude. Firing rate was calculated from the average spike count over 100-ms current pulses. Examples of his data are shown in Fig. 4. Model data are superimposed on to Fig. 4 and show the same monotonicity as the neural data.

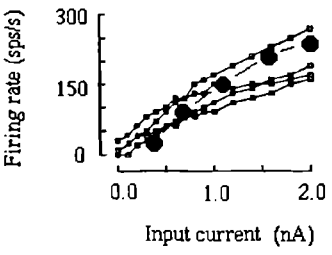

FIG. 4. Average firing rate versus input current. Open squares from DCN neurons (redrawn from Manis, 1990, Fig. 5). Filled circles from model.

D. Changes in temporal response with current bias

The main effect reported by Manis (1990) was that steady-state hyperpolarization altered cell responding to subsequent depolarization. Examples are shown in Fig. 5, top panels. In column A, a current step of 0.5 nA is delivered to the cell following a period of steady-state hyperpolarization at various levels. With no prior hyperpolarization (A1), the cell fires a regular train of action potentials; the latency to firing is less than 10 ms. With increasing levels of prehyperpolarization the latency to firing increases (A2, A3, etc.). Steady-state prehyperpolarization to 20 mV below resting potential (A5) prevents firing until about 90 ms into the depolarizing pulse. Column B shows the data gathered from a similar experimental protocol except that a depolarizing pulse of 1.0 nA is delivered to the cell after the period of hyperpolarization. With no prior hyperpolarization (B1) the cell fires a train of action potentials. With increasing levels of prior hyperpolarization (B2, B3, etc.), the first interspike interval increases.

Figure 5, bottom panels show data gathered from the model using the same protocol as above. Column A shows responses to a depolarizing current pulse of 0.31 nA following increasing levels of steady-state hyperpolarization. Column B shows responses where the depolarizing pulse is stepped to 0.55 nA following the hyperpolarization. The model responses are qualitatively similar to the neural data.

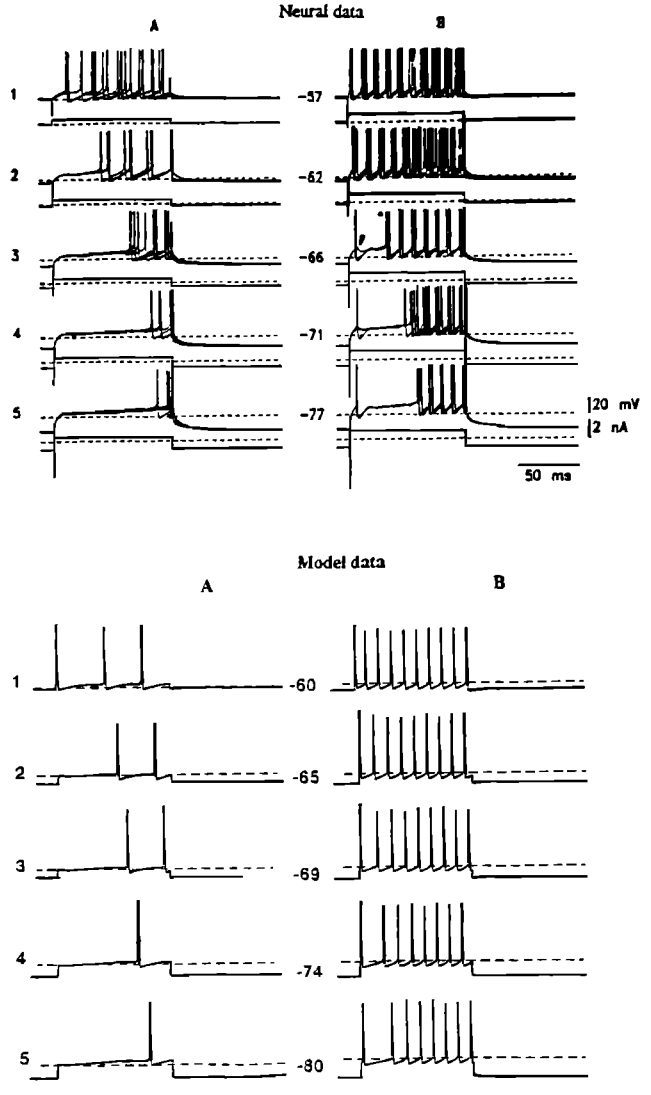

FIG. 5. Neural and model responses to prehyperpolarization–depolarization protocol. Neural data (redrawn from Manis, 1990 Fig. 8) show superimposition of 3–4 traces for each stimulus condition. Figures between columns indicate the cell potential prior to depolarizing pulse. See text for details.

E. Effects of changing model parameters

The Hodgkin–Huxley equation system consists of a number of complex, nonlinear, interacting components. The effect of changing single model parameters on model output is equally complex and depends on the initial configuration of the model. However, given the standard set of parameters (see the Appendix), some of the more pertinent changes and their effects are documented below.

The first demonstrations show the effects of removing the transient potassium conductance from the model (i.e., $\bar{g}_A$=0.0). This equates to the original Hodgkin–Huxley model but with parameter changes. Figure 6(a) shows the model's response to a 100-ms depolarizing current pulse; a series of stereotyped action potentials results. The average firing rate to current pulses of differing magnitudes is shown in Fig. 6(b). The data show a rather small range of spike rates compared to those shown in Fig. 4. The limited dynamic range of the original Hodgkin–Huxley model has long been documented (e.g., Shapiro and Lenherr, 1972). The addition of the transient potassium conductance to the model serves to extend the dynamic range of the model. We shall return to this issue later. The model's response to a depolarizing current pulse following prehyperpolarization (not shown) was no different from that elicited when no prehyperpolarization was imposed.

The next sequence of outputs relate to changes in the parameters that govern the transient potassium conductance. Figure 7 shows the effect of reducing the time constant of the conductance's inactivation, τ_B. The parameter is an important determinant of the latency to the first spike (and the duration of the first interspike interval) in response to the stimulus protocols described above. Other parameters also influence the model's response to the above stimulus paradigm. For instance, reducing $\bar{g}_A$ reduced latency to first spike (not shown). Figure 8 shows that shifts in the conductance's activation and inactivation functions also alter model responses. These will be discussed further in Sec. III below.

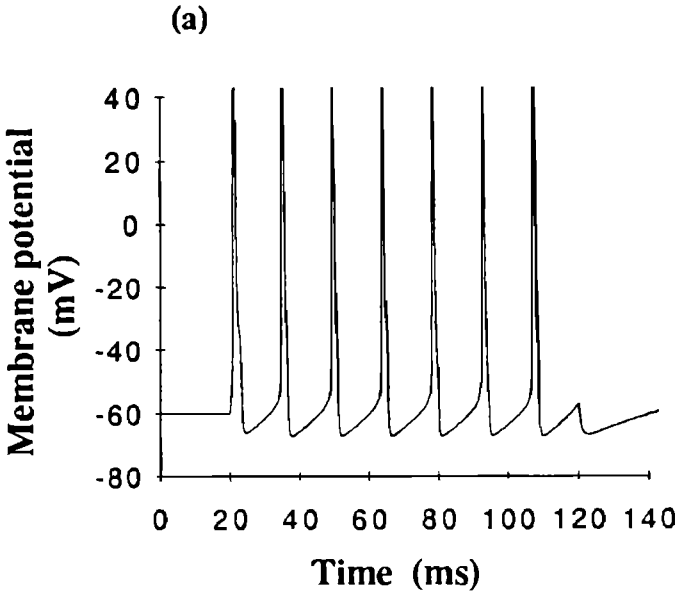

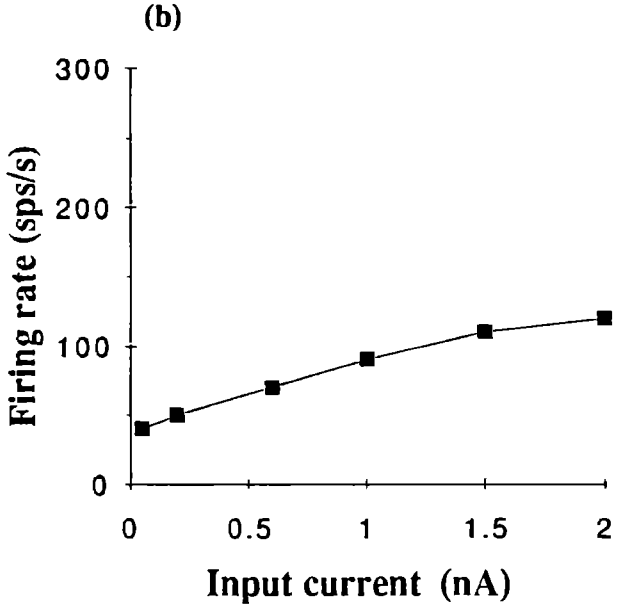

FIG. 6. Model data with g_A=0.0 (g_L=0.31 and I_{Fac}=20). (a) Response to a depolarizing current pulse, 0.6 nA, onset at t=20 ms, duration 100 ms. (b) Average firing rate versus input current.

Variation of the conductance's activation time constant, τ_A, also produced changes in the model's output. The most notable effect concerns the change in the model's response to the onset of hyperpolarizing pulses (not shown). By reducing the time constant two effects were noted. First, the time course of the initial onset response was reduced. Second, the initial onset response was slightly increased and the sag in the membrane trajectory to a steady-state potential became slightly more prominent. The combined effect produced outputs *quantitatively* similar to those recorded by Manis [e.g., redrawn in Fig. 2(c), −1.0-nA input].

III. DISCUSSION

We have presented and evaluated a computer model of the intrinsic membrane properties of DCN pyramidal neu-

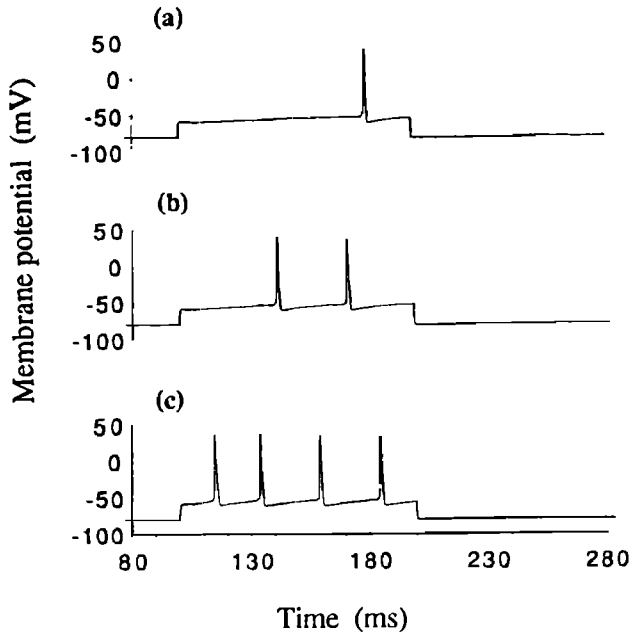

FIG. 7. Effect of varying inactivation time constant, B on model output to stimulus protocol of Fig. 5. (a) B_{fac}=7, i.e., as Fig. 5 panel A5. (b) B_{fac}=5. (c) B_{fac}=3.

rons. The model was cast in terms of the Hodgkin–Huxley (1952) equations of spike generation. The basic model consisted of the standard sodium and potassium ion conductances together with a fixed leakage conductance and a fixed capacitance. Additional to the basic model was a transient potassium conductance (the "A" conductance described by Connor and Stevens, 1971). This addition enabled us to re-

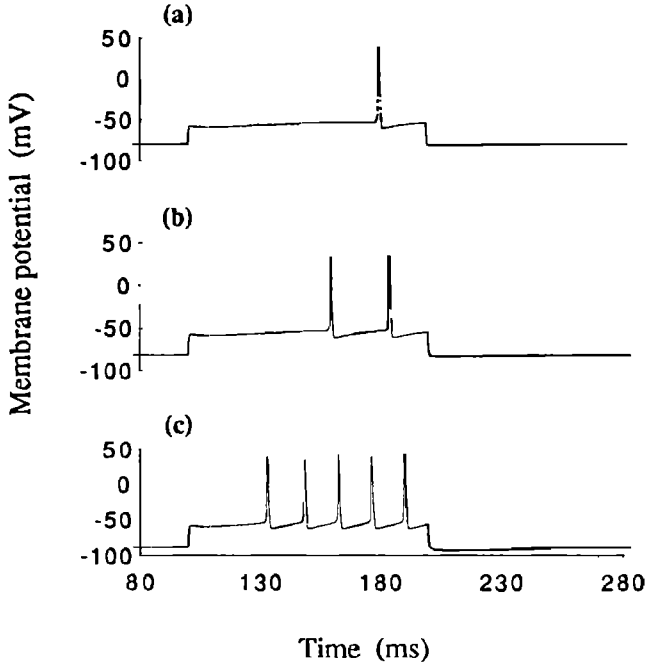

FIG. 8. Effect of varying activation and inactivation functions, A_∞ and B_∞, on model output to stimulus protocol of Fig. 5. (a) A_{SH}=−0.2, B_{SH}=−1.0, (g_L=2.81), i.e., as Fig. 5 panel A5; (b) A_{SH}=−5.0 (g_L=2.49); (c) B_{SH}=−5.0 (g_L=3.94).

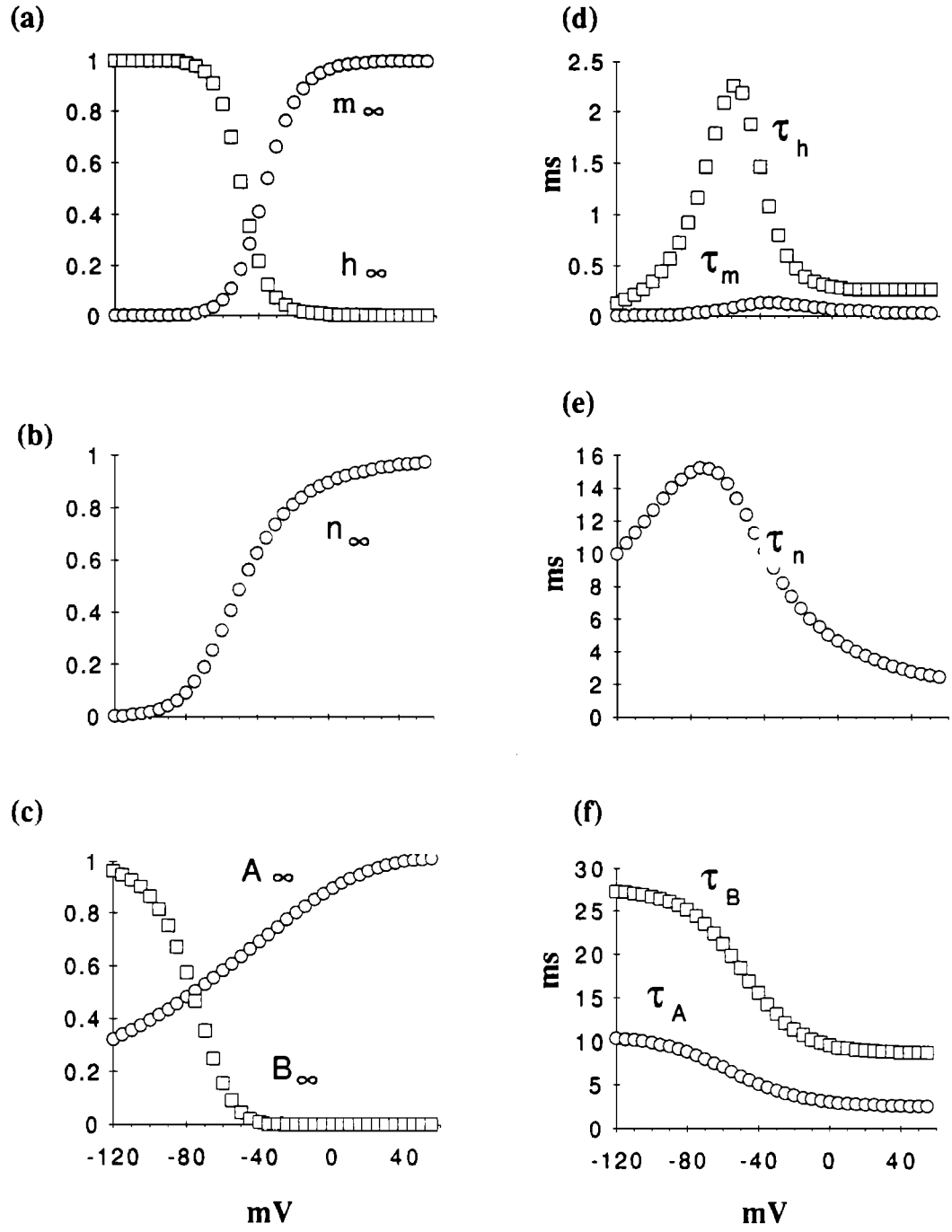

FIG. 9. (a)–(c) Model activation and inactivation parameters for sodium, potassium (activation only) and transient potassium conductances. (d)–(f) corresponding time constants.

produce the generation of pauser and build-up response profiles in a manner consistent with DCN pyramidal cells studied *in vitro*.

The model corroborates the theory of Manis (1990) and others (Rhode *et al.*, 1983) that the response profile of these cells to acoustic stimuli *in vivo* may be determined by prior steady-state hyperpolarization of the cell membrane. The hyperpolarization could be maintained by one of many inhibitory sources that make synaptic contact with these cells (e.g., Smith and Rhode, 1985). Moreover, the model supports the suggestion of Manis (1990) that intrinsic membrane conductances, particularly the "*A*" conductance, play a major role in shaping the cell responses in these circumstances.

An insight into the mechanism that underlies the responses can be gleaned from the model. First, we describe the sequence of events during the simulation of an action potential using the original Hodgkin–Huxley formulation. We then consider the events when the transient potassium conductance is added to the model. Finally, we describe how the addition of the transient potassium conductance underpins the generation of the salient features presented in Fig. 5. The descriptions will be cast in terms of membrane conductances and the activation and inactivation functions that govern them. As an aid to these descriptions, reference will be made to the functions used by the model. The functions,

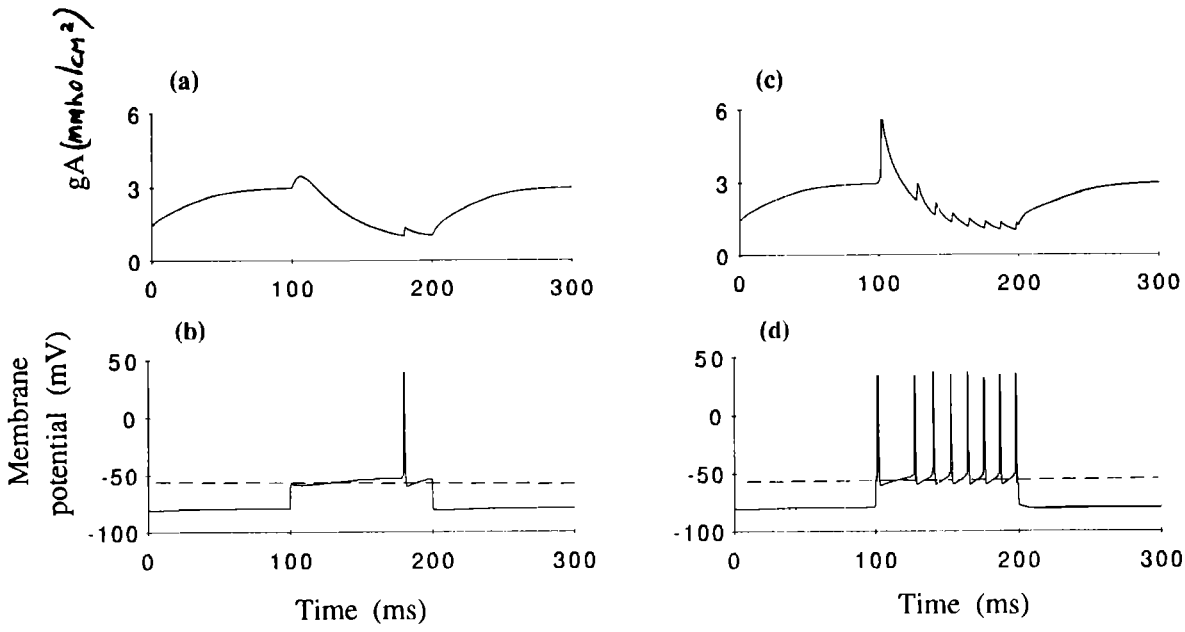

FIG. 10. Model responses to stimulus protocol of Fig. 5. (a) and (b) show g_A and membrane potential, respectively, as a function of time in response to 100 ms depolarizing pulse (0.31 nA) preceded, and followed by 100-ms hyperpolarizing pulse (−1.2 nA). (c) and (d) as above but depolarizing pulse stepped to 0.55 nA. Dotted line denotes cell resting potential (−60 mV).

shown in Fig. 9, were generated using the standard parameter set (see Appendix).

Simulation of positive current applied to the original Hodgkin–Huxley model causes depolarization of the membrane. The rise in membrane potential increases the activation of the sodium conductance (function m_∞, Fig. 9), allowing the rapid entry of positive ions into the cell. During the upward swing in membrane potential the sodium conductance becomes inactivated (function h_∞), and the potassium conductance becomes activated (function n_∞); the inward flow of sodium ions slows and the outward flow of potassium ions increases. At the peak of the action potential, these two currents are equal. After this point, the potassium current exceeds the sodium current, and the membrane potential rapidly returns toward the resting level and beyond. The large potassium conductance resulting from the spike hyperpolarizes the cell. Given the long time constant of the potassium conductance in this voltage region (τ_n, Fig. 9), the membrane potential recovers only slowly back to resting potential. The hyperpolarization of the membrane and its subsequent recovery constitute the refractory period of the cell.

The above sequence of events is modified by the addition of the transient potassium conductance. Initially, as the membrane starts to depolarize, g_A is activated [Fig. 9(c) function A_∞] and an outward potassium current flows which opposes the applied current. This has the effect of slowing the rate of depolarization to the first spike. Postspike hyperpolarization of the membrane also activates g_A which gives a longer recovery process. This leads to increased interspike intervals and, therefore, a reduction in the firing rate. For stronger input pulses, the rise in g_A is increasingly by-passed as the membrane potential moves more rapidly through its voltage range of activation. In all, this mechanism serves to overcome the limited dynamic range of the original Hodgkin–Huxley model [compare Figs. 4 and 6(b)].

The effect of prehyperpolarization on pyramidal cell membranes and their subsequent responses to depolarization can also be explained by reference to the transient potassium conductance. The first part of this account follows closely that originally described by Connor and Stevens (1971) for the gastropod neuron somata.

At membrane potentials below resting (−60 mV in this case), the transient potassium conductance increases. This is largely due to the *deinactivation* of the function B_∞ [see Fig. 9(c)]. Steady-state hyperpolarization, therefore, places the membrane in a state where, on depolarization, the effects of g_A will be more pronounced than those at normal resting levels. Figure 10(a) shows a temporal version of these events. Figure 10(b) shows the response of the model cell to the stimulus protocol used in Fig. 5, model data A5. The slow rise in membrane potential to the spike is governed by the depolarizing current pulse which is tempered by the slow inactivation of the transient potassium conductance [note from Fig. 9(f) that τ_B is about 25–30 ms at voltages just below resting].

The second case is where the depolarizing pulse is sufficient to overcome the increased g_A [Fig. 10(c) and (d)]. The pulse gives rise to an action potential at onset. As g_A is voltage-dependent, it becomes further activated by this event. The spike-induced activation of g_A is added to that already produced by the period of hyperpolarization. The interval to the next spike is, therefore, increased as g_A slowly becomes inactivated from its raised state.

Within this descriptive framework it is possible to explain the main data presented by Manis (1990, redrawn in Fig. 5 above). Additionally, it is possible to understand the effects of the various parameter changes made in Sec. II E above. A reduction in the time constant of inactivation will

lead to a reduction in the latency to spiking (Fig. 7); a reduction in the conductance's normalization factor, $\bar{g}_A$, will have a similar effect (not shown). Finally, the position of the activation and inactivation functions along the voltage axis will determine exactly how the model responds to the prehyperpolarization-depolarization paradigm (Fig. 8).

IV. CONCLUSIONS

We have presented and evaluated a model of the intrinsic properties of DCN pyramidal cells. The salient features of this class of cells can be replicated by the addition of a transient potassium conductance to Hodgkin–Huxley formulation of spike generation in neuronal tissue. However, a fuller understanding of the DCN must await studies which consider the complex interactions of inputs to these cells from outside the nucleus and from those within. It is likely that computer models, such as the one presented here, will play a strategic role in this research.

ACKNOWLEDGMENTS

This research was supported by a Basic Research grant from the Esprit programme of the European Community (BRA grant SSS 6961), and an equipment grant from Apple Computers Inc., USA. We thank the three anonymous reviewers who provided helpful comments on an earlier version of this paper.

APPENDIX

The principal differential equation describing the circuit of Fig. 1 is

$$I(t)=C_M\frac{dV}{dT}+g_L(V-E_L)+g_{\mathrm{Na}}(V-E_{\mathrm{Na}})+g_{\mathrm{K}}(V-E_{\mathrm{K}})+g_A(V-E_A)+I_{\mathrm{soma}}. \quad \text{(A1)}$$

1. Sodium conductance

The sodium conductance g_{Na} is a function of both membrane potential V and time t.

$$g_{\mathrm{Na}}=\bar{g}_{\mathrm{Na}}m^3(V,t)h(V,t), \quad \text{(A2)}$$

where $\bar{g}_{\mathrm{Na}}$ is a normalization conductance factor, and $m(V,t),h(V,t)\in(0,1)$ are the activation and inactivation functions, respectively. The function m is the solution to the first-order differential equation

$$\tau_m\frac{dm}{dt}+m=m_\infty, \quad \text{(A3)}$$

where

$$\tau_m=M_{\mathrm{fac}}\frac{1}{(\alpha_m+\beta_m)}, \quad \text{(A4)}$$

$$m_\infty=\frac{\alpha_m}{\alpha_m+\beta_m}, \quad \text{(A5)}$$

and

$$\alpha_m=\frac{-0.1(V+37+M_{SH})}{\exp\{[-(V+37+M_{SH})]/10\}-1}, \quad \text{(A6)}$$

$$\beta_m=4\exp\left(\frac{-(V+62+M_{SH})}{18}\right). \quad \text{(A7)}$$

Similarly, h is defined as

$$\tau_h\frac{dh}{dt}+h=h_\infty, \quad \text{(A8)}$$

where

$$\tau_h=H_{\mathrm{fac}}\frac{1}{(\alpha_h+\beta_h)}, \quad \text{(A9)}$$

$$h_\infty=\frac{\alpha_h}{\alpha_h+\beta_h}, \quad \text{(A10)}$$

and

$$\alpha_h=0.07\exp\left(\frac{-(V+62+H_{SH})}{20}\right), \quad \text{(A11)}$$

$$\beta_h=\left[\exp\left(\frac{-(V+32+H_{SH})}{10}\right)+1\right]^{-1}. \quad \text{(A12)}$$

Following the practice of Connor *et al.* (1977) and Banks and Sachs (1991), the m and h parameters were adjusted to give realistic spike threshold values. Here, m was moved -0.3 mV to the right on the voltage axis ($M_{SH}=-0.3$) and h was moved 10 mV to the right ($H_{SH}=-10.0$). The sodium equilibrium potential, $E_{\mathrm{Na}}=55$ mV and $\bar{g}_{\mathrm{Na}}=120$ mmho/cm^2. $M_{\mathrm{fac}}=0.263$, $H_{\mathrm{fac}}=0.263$.

2. Delayed potassium conductance

The delayed rectifier potassium conductance is a function of both V and t

$$g_k=\bar{g}_k n^4(V,t). \quad \text{(A13)}$$

The function n is the solution to the first-order differential equation

$$\tau_n\frac{dn}{dt}+n=n_\infty, \quad \text{(A14)}$$

where

$$\tau_n=N_{\mathrm{fac}}\frac{1}{(\alpha_n+\beta_n)}, \quad \text{(A15)}$$

$$n_\infty=\frac{\alpha_n}{\alpha_n+\beta_n}, \quad \text{(A16)}$$

and

$$\alpha_n=\frac{-0.01(V+52+N_{SH})}{\exp\{[-(V+52+N_{SH})]/10\}-1}, \quad \text{(A17)}$$

$$\beta_n=0.125\exp\left(\frac{-(V+62+N_{SH})}{80}\right), \quad \text{(A18)}$$

n was moved 1.3 mV to the right on the voltage axis ($N_{SH}=-1.3$). The potassium equilibrium potential, $E_{\mathrm{K}}=-72$ mV and $\bar{g}_{\mathrm{K}}=36$ mmho/cm^2. $N_{\mathrm{fac}}=2.63$. [N.B. We have not implemented the voltage-dependent scaling factor on the potassium activation time constant as used by Banks and Sachs (1991).]

3. Transient potassium conductance

The transient potassium conductance g_A was implemented exactly as stated in Connor *et al.* (1977)

$$g_A=\bar{g}_A A^3(V,t)B(V,t). \tag{A19}$$

The factors A and B have the same functional significance as the m and h factors of the sodium conductance system. That is

$$\tau_A \frac{dA}{dt}+A=A_\infty, \tag{A20}$$

where

$$\tau_A=A_{\text{fac}}\left(0.3632+\frac{1.158}{1+\exp\{(V+55.96+A_{SH})/20.12\}}\right), \tag{A21}$$

$$A_\infty=\left(0.0761\,\frac{\exp\{(V+94.22+A_{SH})/31.84\}}{1+\exp\{(V+1.17+A_{SH})/28.93\}}\right)^{1/3}, \tag{A22}$$

and

$$\tau_B \frac{dB}{dt}+B=B_\infty, \tag{A23}$$

where

$$\tau_B=B_{\text{fac}}\left(1.24+\frac{2.678}{1+\exp\{(V+50.0+B_{SH})/16.027\}}\right), \tag{A24}$$

$$B_\infty=\frac{1}{\{1+\exp[(V+53.3+B_{SH})/14.54]\}^4}. \tag{A25}$$

Simulations were run with $A_{SH}=-0.2$, $B_{SH}=-1.0$, $A_{\text{fac}}=7.0$, $B_{\text{fac}}=7.0$, $\bar{g}_A=47.4$ mmho/cm^2 and $E_A=-72$ mV.

4. Capacitance and leakage current

$C_M=1$ μF/cm^2 and $g_L=2.8$ mmho/cm^2. The leakage equilibrium potential $E_L=-53$ mV.

5. Input current

I_{soma} represents the magnitude of the current (in nA) injected into the cell soma. All input values used in this study were multiplied by a scaling factor, $I_{\text{fac}}=80$.

[1]The model equations were incorporated into the LUTEar Core Routines Library (CRL). The CRL comprises software modules developed by the Speech and Hearing Laboratory at Loughborough to simulate auditory processing. The compressed archive of CRL is available via anonymous FTP: sun.lut.ac.uk: /public/hulpo. It is available in Unix, Macintosh and MS-DOS formats.

Adams, J. C. (**1976**). "Single unit studies on the dorsal and intermediate acoustic striae," J. Comp. Neurol. **170**, 97–106.

Arle, J. E., and Kim, D. O. (**1991**). "Neural modeling of intrinsic and spike-discharge properties of cochlear nucleus neurons," Biol. Cyber. **64**, 273–283.

Banks, M. I., and Sachs, M. B. (**1991**). "Regularity analysis in a compartmental model of chopper units in the anteroventral cochlear nucleus," J. Neurophysiol. **65**, 606–629.

Britt, R., and Starr, A. (**1976**). "Synaptic events and discharge patterns of cochlear nucleus cells. I. Steady-frequency tone bursts," J. Neurophysiol. **39**, 162–178.

Connor, J. A., and Stevens, C. F. (**1971**). "Prediction of repetitive firing behaviour from voltage clamp data on an isolated neurone soma," J. Physiol. (London) **213**, 31–53.

Connor, J. A., Walter, D., and McKown, R. (**1977**). "Neural repetitive firing: Modifications of the Hodgkin–Huxley axon suggested by experimental results from crustacean axons," Biophys. J. **18**, 81–102.

Ghoshal, S., Kim, D. O., and Northrop, R. B. (**1992**). "Amplitude-modulated tone encoding behavior of cochlear nucleus neurons: Modeling study," Hear. Res. **58**, 153–165.

Godfrey, D. A., Kiang, N. Y. S., and Norris, B. E. (**1975**). "Single unit activity in the dorsal cochlear nucleus of the cat," J. Comp. Neurol. **162**, 269–284.

Goldberg, J. M., and Brownell, W. E. (**1973**). "Discharge characteristics of neurons in the anteroventral and dorsal cochlear nuclei of cat," Brain Res. **64**, 35–54.

Greenwood, D. D., and Maruyama, N. (**1965**). "Excitatory and inhibitory response areas of auditory neurons in the cochlear nucleus," J. Neurophysiol. **28**, 863–892.

Hewitt, M. J., and Meddis, R. (**1993**). "Regularity of cochlear nucleus stellate cells: A computational modeling study," J. Acoust. Soc. Am. **93**, 3390–3399.

Hewitt, M. J., and Meddis, R. (**1994**). "A computer model of amplitude modulation sensitivity of single units in the inferior colliculus," J. Acoust. Soc. Am. **95**, 2145–2159.

Hewitt, M. J., Meddis, R., and Shackleton, T. M. (**1992**). "A computer model of a cochlear nucleus cell: Responses to pure-tone and amplitude-modulated stimuli," J. Acoust. Soc. Am. **91**, 2096–2109.

Hirsch, J. A., and Oertel, D. (**1988a**). "Intrinsic properties of neurons in the dorsal cochlear nucleus of mice *in vitro*," J. Physiol. (London) **396**, 535–548.

Hirsch, J. A., and Oertel, D. (**1988b**). "Synaptic connections in the dorsal cochlear nucleus of mice *in vitro*," J. Physiol. (London) **396**, 549–562.

Hodgkin, A. L., and Huxley, A. F. (**1952**). "A quantitative description of membrane current and its application to conduction and excitation in nerve," J. Physiol. (London) **117**, 500–544.

Kane, E. C. (**1974**). "Synaptic organization in the dorsal cochlear nucleus of the cat: A light and electron microscope study," J. Comp. Neurol. **155**, 301–330.

MacGregor, R. J. (**1987**). *Neural and Brain Modeling* (Academic, San Diego).

Manis, P. B. (**1990**). "Membrane properties and discharge characteristics of guinea pig dorsal cochlear nucleus neurons studied *in vitro*," J. Neurosci. **10**, 2338–2351.

Rhode, W. S., and Kettner, R. E. (**1987**). "Physiological study of neurons in the dorsal and anteroventral cochlear nucleus of the unanesthetized cat," J. Neurophysiol. **56**, 287–307.

Rhode, W. S., and Smith, P. H. (**1986**). "Physiological studies on neurons in the dorsal cochlear nucleus of the cat," J. Neurophysiol. **56**, 287–307.

Rhode, W. S., Smith, P. H., and Oertel, D. (**1983**). "Physiological response properties of cells labeled intracellularly with horseradish perioxidase in cat dorsal cochlear nucleus," J. Comp. Neurol. **213**, 426–447.

Romand, R. (**1978**). "Survey of intracellular recording in the cochlear nucleus of the cat," Brain Res. **148**, 43–65.

Shapiro, B. I., and Lenherr, F. K. (**1972**). "Hodgkin–Huxley axon: Increased modulation and linearity of response to constant current stimulus," Biophys. J. **12**, 1145–1158.

Smith, P. H., and Rhode, W. S. (**1985**). "Electron microscope features of physiologically characterized, HRP-labelled fusiform cells in the cat dorsal cochlear nucleus," J. Comp. Neurol. **237**, 127–143.

Smith, P. H., and Rhode, W. S. (**1989**). "Structural and functional properties distinguish two types of multipolar cells in the ventral cochlear nucleus," J. Comp. Neurol. **282**, 595–616.